European Journal of Nuclear Medicine and Molecular Imaging (2018) 45:787–797
https://doi.org/10.1007/s00259-017-3896-9

ORIGINAL ARTICLE

Superiority of ^{68}Ga-DOTATATE over ^{18}F-FDG and anatomic imaging in the detection of succinate dehydrogenase mutation (*SDHx*)-related pheochromocytoma and paraganglioma in the pediatric population

Abhishek Jha[1] · Alexander Ling[2] · Corina Millo[3] · Garima Gupta[1] · Bruna Viana[1] · Frank I. Lin[4] · Peter Herscovitch[3] · Karen T. Adams[1] · David Taïeb[5] · Adam R. Metwalli[6] · W. Marston Linehan[6] · Alessandra Brofferio[7] · Constantine A. Stratakis[8] · Electron Kebebew[9] · Maya Lodish[8] · Ali Cahid Civelek[10] · Karel Pacak[1]

Received: 22 July 2017 / Accepted: 21 November 2017 / Published online: 4 December 2017

Abstract

Purpose To evaluate and compare diagnostic performance of ^{68}Ga-DOTA(0)-Tyr(3)-octreotate (^{68}Ga-DOTATATE) with ^{18}F–fluoro-2-deoxy-D-glucose (^{18}F–FDG) positron emission tomography-computed tomography (PET/CT) and anatomic imaging using computed tomography and/or magnetic resonance (CT/MR) imaging in detection of *SDHx*-related pheochromocytomas and paragangliomas (PPGLs) in pediatric patients.

Methods Nine pediatric patients (5:4, girls:boys; 14.6 ± 2.0 years) with an *SDHx*-related mutation (*SDHB*:*SDHA*:*SDHD*, $n = 7:1:1$) were included in this retrospective study. At the time of initial diagnosis, 7/9 patients had metastatic disease. They underwent CT/MR imaging along with PET/CT using ^{68}Ga-DOTATATE ($n = 9$), ^{18}F–FDG ($n = 8$), and positron emission tomography-magnetic resonance imaging (PET/MR) using ^{18}F–FDG ($n = 1$). In this manuscript, ^{18}F–FDG PET/CT refers to both ^{18}F–FDG PET/CT and ^{18}F–FDG PET/MR. The per-lesion, per-region, and per-patient detection rates were compared and calculated for each of the imaging modalities. A composite of all functional and anatomic imaging studies served as the imaging comparator.

Results Eight out of nine patients were positive for PPGLs on the imaging studies that demonstrated 107 lesions in 22 anatomic regions on the imaging comparator. The per-lesion detection rates for ^{68}Ga-DOTATATE PET/CT, ^{18}F–FDG PET/CT, and CT/MR imaging were 93.5% (95%CI, 87.0% to 97.3%); 79.4% (95%CI, 70.5% to 86.6%); and 73.8% (95%CI, 64.5% to 81.9%), respectively. The per-lesion detection rate for ^{68}Ga-DOTATATE PET/CT was significantly higher than that of ^{18}F–FDG PET/CT ($p = 0.001$) or CT/MR imaging ($p < 0.001$). In all of the anatomic regions except abdomen, the per-lesion detection rates for ^{68}Ga-

Ali Cahid Civelek and Karel Pacak equally share the senior authorship.

✉ Karel Pacak
karel@mail.nih.gov

[1] Section on Medical Neuroendocrinology, Eunice Kennedy Shriver National Institute of Child Health and Human Development, National Institutes of Health, 10 Center Dr., Bldg. 10, Room 1E-3140, Bethesda, MD 20892, USA

[2] Radiology and Imaging Sciences, Warren Grant Magnuson Clinical Center, National Institutes of Health, 10 Center Dr., Bldg. 10, Bethesda, MD 20892, USA

[3] Positron Emission Tomography Department, Warren Grant Magnuson Clinical Center, National Institutes of Health, 10 Center Dr., Bldg. 10, Room 1C-401 and 490, Bethesda, MD 20892, USA

[4] Molecular Imaging Program, National Cancer Institute, National Institutes of Health, 10 Center Dr., Bldg. 10, Room B3B69F, Bethesda, MD 20892, USA

[5] Department of Nuclear Medicine, La Timone University Hospital, CERIMED, Aix-Marseille University, Marseille, France

[6] Urologic Oncology Branch, National Cancer Institute, National Institutes of Health, Bldg. 10, Room 2 W-5940 and Room 1-5940, 10 Center Drive, Bethesda, MD 20892, USA

[7] Cardiovascular & Pulmonary Branch, National Heart Lung and Blood Institute, National Institutes of Health, 10 Center Dr., Bldg. 10, Room 5-3130, Bethesda, MD 20892, USA

[8] Section on Endocrinology and Genetics, Eunice Kennedy Shriver National Institute of Child Health and Human Development, National Institutes of Health, 10 Center Dr., Bldg. 31, Room 2A46 and Bldg. 10, Room 2-5142, Bethesda, MD 20892, USA

[9] Endocrine Oncology Branch, Center for Cancer Research, National Cancer Institute, 10 Center Dr., Bldg. 10, Room 4-5952, Bethesda, MD 20892, USA

[10] Nuclear Medicine Division, Radiology and Imaging Sciences, Warren Grant Magnuson Clinical Center, National Institutes of Health, 10 Center Dr., Bldg. 10, Room 1C-455, Bethesda, MD 20892, USA

DOTATATE PET/CT was found to be equal or superior to ^{18}F–FDG PET/CT, and CT/MR imaging. The per-region detection rate was 100% (95%CI, 84.6% to 100%) for ^{68}Ga-DOTATATE PET/CT and 90.9% (95%CI, 70.8% to 98.9%) for both ^{18}F–FDG PET/CT and CT/MR imaging. The per-patient detection rates for ^{68}Ga-DOTATATE PET/CT, ^{18}FDG PET/CT, and CT/MR imaging were all 100% (95%CI, 63.1% to 100%).

Conclusion Our preliminary study demonstrates the superiority of ^{68}Ga-DOTATATE PET/CT in localization of *SDHx*-related PPGLs in pediatric population compared to ^{18}F–FDG PET/CT and CT/MR imaging with the exception of abdominal (excluding adrenal and liver) lesions, and suggests that it might be considered as a first-line imaging modality in pediatric patients with *SDHx*-related PPGLs.

Keywords ^{68}Ga-DOTATATE · FDG · PET/CT · Pediatric · Pheochromocytoma · Paraganglioma

Introduction

Pheochromocytomas and paragangliomas (PPGLs) are rare neuroendocrine tumors (NETs) that may occur anywhere along the sympathetic or parasympathetic nervous system, extending from skull base to pelvic floor [1].

Mutations in gene-encoding subunits of succinate dehydrogenase (*SDHx*) or factors necessary for correct assembly of the SDH complex result in several familial PPGL syndromes [2–7]. Malignant transformation is more common in patients with *SDHx* and especially in those related to *SDHB* mutations [8, 9] compared with the other genetic mutations [10–12], resulting in higher mortality and morbidity rates due to more commonly occurring metastases [13].

The incidence of PPGLs in the pediatric population is estimated to be 0.2–0.3 cases per million children [14], whereas the incidence of malignant PPGLs is 0.02 cases per million children [15]. PPGLs in the pediatric population are usually symptomatic, extra-adrenal, likely to be bilateral, and potentially life-threatening [16, 17]. Moreover, a higher rate of *SDHB*-related metastatic disease is found in children than in adults [18]. Therefore, in patients with *SDHx*-related PPGLs, early detection and monitoring of potential metastases is essential to improve clinical management and overall prognosis.

The detection and precise localization of the primary and metastatic PPGL lesions is vital in the decision-making process regarding surgery, radiotherapy or peptide receptor radionuclide therapy (PRRT) [6]. However, the clinical experience, knowledge and understanding of the imaging characteristics of such rare pediatric tumors is extremely limited. Since the pediatric patient population is more likely to be susceptible to radiation-induced late effects [19, 20], radiation exposure from functional and/or anatomic diagnostic imaging should be minimized. Reduction in the diagnostic imaging related radiation dose can be achieved by tracking cumulative radiation dose, as well as adopting a policy to keep the diagnostic test induced cumulative radiation doses to a minimum, as low as reasonably achievable (ALARA) and at the same time not being harmful to the patients due to suboptimal follow-up resulting in missing ideal time for treatment to be initiated. Therefore, in children, it is essential to choose and administer carefully diagnostic imaging studies by using evidence-based performance characteristics of each anatomic and functional imaging modality for the management of these tumors. Recent guidelines from the Endocrine Society recommend MR imaging as the preferred modality in pediatric patients and patients with metastatic disease [21]. They further suggest utilization of ^{18}F–FDG PET/CT as the preferred functional imaging modality in patients with metastatic disease [21]. However, these guidelines did not include the more efficient or successful imaging modalities used to detect metastatic PPGLs, especially recent publications show that in adult patients, the performance of ^{68}Ga-DOTATATE is superior to other imaging tracers such as ^{18}F–FDG, ^{18}F–fluorodopa, and ^{18}F–fluorodopamine in localizing *SDHB*-related metastatic PPGLs [22]. On the other hand, the performance of ^{68}Ga-DOTATATE PET/CT in pediatric *SDHx*-related PPGLs is currently unknown. Furthermore, ^{68}Ga-DOTATATE is now approved for localizing NETs in both adults and pediatric patients by U.S. Food and Drug Administration [23]. Thus, we hypothesized that ^{68}Ga-DOTATATE PET/CT would improve the management of PPGLs in pediatric patients by detecting and localizing PPGLs more accurately.

The purpose of this study was to evaluate and compare the diagnostic performance of ^{68}Ga-DOTATATE PET/CT, ^{18}F–FDG PET/CT and anatomic (CT/MR) imaging in detection of *SDHx*-related PPGLs in pediatric population.

Materials and methods

Patients

The flow chart of the study cohort describing the 17 consecutive pediatric patients who underwent ^{68}Ga-DOTATATE PET/CT scans from May 2015 to February 2017 is provided in Fig. 1.

In this retrospective study of the 17 patients, a total of 9 unrelated *SDHx* pediatric patients who were 10–18 years old at the time of functional and anatomic imaging were included. There were five girls and four boys with a mean age of 14.6 ±

2.0 years, and all with *SDHx*-related mutations (*SDHA*, $n = 1$; *SDHB*, $n = 7$; *SDHD*, n = 1) at genetic testing.

The study protocol was approved by the institutional review board of the *Eunice Kennedy Shriver* National Institute of Child Health and Development (ClinicalTrials.gov Identifier: NCT00004847). Informed assent from the patients and signed permission from one or both parents were obtained for all clinical, genetic, biochemical, and imaging studies regarding PPGLs.

We included patients between 10 and 18 years of age with biochemical, histologic and/or imaging evidence of *SDHx*-related PPGLs who have undergone integrated PET/CT or PET/MR functional imaging with ^{68}Ga-DOTATATE and ^{18}F–FDG as well as CT and/or MR imaging. Demographic data, including age at initial diagnosis, age at metastatic disease, genetic mutation, family history, biochemical data and therapeutic interventions were obtained from the electronic medical records.

Mean age at diagnosis of primary PPGL was 12.2 ± 3.0 years. The average duration between diagnosis of a primary tumor and referral to the National Institutes of Health was 2.2 ± 2.2 years. At the time of initial diagnosis, seven out of nine patients were found to have metastatic disease, and the remaining two patients developed metastatic disease after 2 years of initial diagnosis. Eight out of nine patients underwent prior resection of their primary PPGL. The clinical characteristics of individual patients are summarized in Table 1.

Five of the nine patients had both CT and MR studies, two patients received MR imaging only, and the remaining two patients received CT scans only. Two patients received additional dedicated MR imaging of the spine. Eight out of nine patients received anatomic imaging studies at our institution, whereas one patient (Pt. no. 2 in Table 1) presented to us with CT and MR imaging studies performed at an outside institution. Since their image quality was acceptable, to avoid unnecessary additional radiation exposure, those studies were assessed and included in this study, and not repeated.

All nine patients underwent whole body ^{68}Ga-DOTATATE PET/CT scanning. Eight out of nine patients also received ^{18}F–FDG PET/CT studies. The remaining patient (Pt. no. 9 in Table 1) presented to us with a ^{18}F–FDG PET/MR scan performed at an outside institution. To avoid unnecessary additional radiation exposure to this patient, the ^{18}F–FDG PET/MR scan was assessed and included and a ^{18}F–FDG PET/CT scan was circumvented. In this manuscript, ^{18}F–FDG PET/CT refers to both ^{18}F–FDG PET/CT and ^{18}F–FDG PET/MR.

Imaging Studies and Techniques

CT scans of the neck, chest, abdomen, and pelvis were all performed using Siemens Somatom Force scanners, Siemens Medical Solutions except for one set of studies performed at another institution using a Toshiba Aquilion ONE device, Toshiba Medical Systems. Section thickness was 2.0 mm for all studies except for 3.0 mm thickness for the single patient with studies from another institution. All studies were performed with intravenous (i.v.) rapid infusion of nonionic water-soluble contrast agent, as well as oral contrast material. MR scans of the neck, chest, abdomen and pelvis were obtained with 1.5 and 3 Tesla scanners (Philips Achieva 1.5 or 3 Tesla, Philips Medical Systems; Siemens Aera 1.5 Tesla, Siemens Skyra 3 Tesla, Siemens Verio 3 Tesla, Siemens Biograph 3 Tesla, Siemens Medical Solutions). Imaging protocols varied by body part, for the neck including STIR and/or T2-weighted images as well as multiplanar T1-weighted sequences before and after infusion of 0.2 ml/kg of a gadolinium-containing contrast agent. Chest and abdomen studies additionally included multiphase T1-weighted post-injection images, and abdomen and pelvis studies also included diffusion-weighted sequences. Image thickness was at most 5 mm for all neck studies, and at most 6 mm for chest, abdominal, and pelvic scans; post-gadolinium contrast images as thin as 1 mm in the neck, and 3 mm for other body parts were obtained for all but a few scans.

As ^{68}Ga-DOTATATE PET/CT is a research PET scan at the NIH, the ^{68}Ga-DOTATATE PET/CT protocol in children was optimized to reduce the radiation dose, in accordance with the ALARA principle. This includes reducing the administered dose of radiotracer according to the child's weight, as well as reducing the tube current according to the child's size and imaging requirements. For ^{68}Ga-DOTATATE, a fixed dose of 74 MBq for children between 10 and 15 years of age, and a fixed dose of 111 MBq for children older than 15 years was used. The co-registered CT for ^{68}Ga-DOTATATE PET/CT was performed at 34 mAs, because we think this is the lowest dose we can use while maintaining image quality. The effective radiation dose delivered after single administration of ^{68}Ga-DOTATATE PET in 10- and 15-year-old child was 1.0 mSv. PET/CT scans from the upper thighs to the skull were performed 60 min after intravenous injection of a mean administered activity of 107.7 ± 17.0 MBq of ^{68}Ga-DOTATATE and 60 min after 186.11 ± 43.7 MBq of ^{18}F–FDG. For ^{18}F–FDG PET/CT imaging, patients were prepared by covering them with warm blankets and controlling the ambient room temperature. All PET/CT scans were performed on Biograph-mCT (Siemens Medical Solutions) 128 PET/CT scanners whereas the PET/MR scan was performed on Biograph-mmR (Siemens Medical Solutions). PET imaging was performed in three-dimensional mode. PET images were reconstructed on a 256 × 256 image matrix using an iterative reconstruction algorithm provided by the manufacturer, utilizing time of flight. Section thickness for PET and CT portions of ^{68}Ga-DOTATATE PET/CT was 1.5 mm and that for FDG PET/CT was 3.0 mm. Non-enhanced low-dose CT studies were performed and used for attenuation correction and anatomic co-registration.

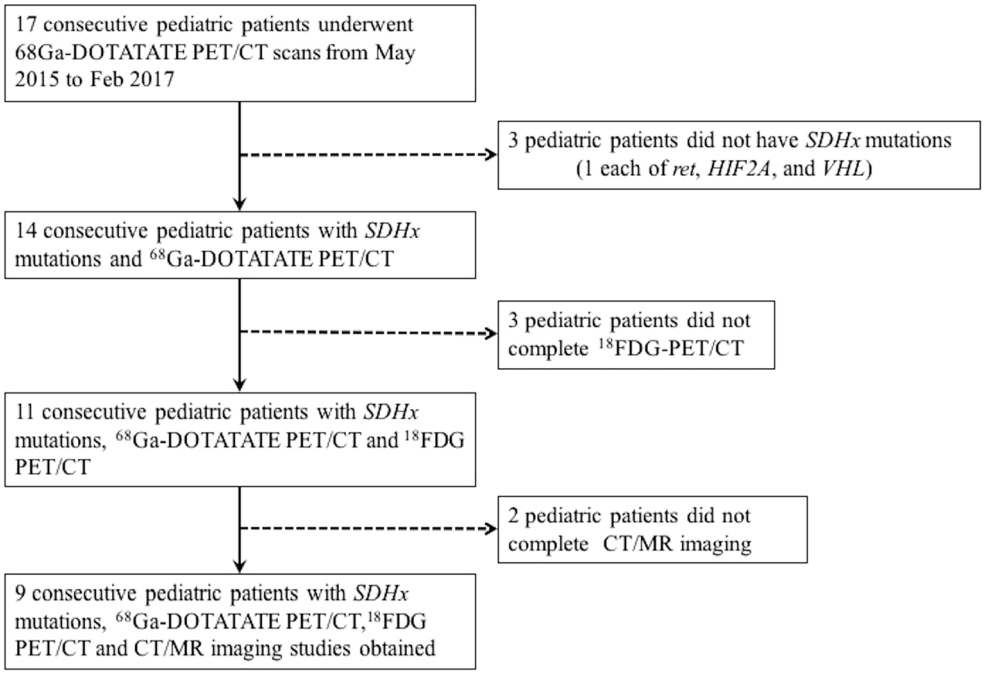

Fig. 1 Study flow chart - description of patient cohort

Analysis of data

All PET/CT and PET/MR studies were interpreted by an experienced nuclear medicine physician and all CT and MR imaging studies were interpreted by an experienced radiologist, who were blinded to all other imaging and clinical data except for the initial diagnosis, sex and age of the patient.

Maximal standardized uptake values (SUV_{max}) were determined from the PET images. Focal areas of non-physiologic increased radiotracer activity with a higher SUV_{max} than the surrounding tissue were considered as lesions.

The median interval between ^{68}Ga-DOTATATE and ^{18}F–FDG PET/CT studies was 3 days (range: 1–185 days), and only one patient had these studies >1 month apart. The median interval between ^{68}Ga-DOTATATE PET/CT and CT/MR imaging studies was 2 days (range: 1–196 days), and only one patient had these studies >1 month apart. For regional analysis, adrenal glands, liver, abdominal/pelvic (excluding adrenal glands and liver), lungs, mediastinum, neck, and bone were analyzed separately.

A patient or region was considered as abnormal or "positive" regardless of the number of positive lesions present. Utilizing all imaging studies, patient-to-patient, region-to-region, and lesion-to-lesion analyses were performed and compared. If the number of lesions in a region exceeded 15, the count was truncated at 15 [22]. The lesions that were not in the imaging field of view of all the imaging modalities were excluded from the analysis. Histologic proof of metastatic lesions was not feasible for all of the metastatic lesions. The composite of anatomic and all performed functional imaging studies was considered the imaging comparator. A "positive" result on any of the imaging studies, i.e. functional imaging and/or CT, and/or MR imaging was counted as true positive for the presence of the disease.

Statistics

Results are given as means with 95% confidence intervals (CIs) unless stated otherwise. For statistical analysis, the McNemar's test was used to compare sensitivities between the different imaging modalities. A two-sided $p < 0.05$ was considered as statistically significant.

Results

Eight out of nine patients were positive according to the imaging comparator, with abnormalities detected on ^{68}Ga-DOTATATE PET/CT, ^{18}F–FDG PET/CT, and/or CT/MR imaging. One patient (Pt. no. 6 in Table 1) was found to have no abnormality on any of the imaging studies. On biochemical evaluation, his catacholamines, metanephrines, and methoxytyramine levels were found to be within normal limits except elevated chromogranin A (1.4 times the upper limit). On follow up evaluation he was found to be free of any detectable tumors on imaging and biochemistry.

^{68}Ga-DOTATATE PET/CT detected 100 of the 107 total lesions identified by the imaging comparator, corresponding to 93.5% of lesions (95% CI, 87.0% to 97.3%) with a mean SUV_{max} of 27.6 ± 29.5 (median: 19.4; range: 2.2 to 177). This was significantly higher than the 85 of the 107 lesions detected by ^{18}F–FDG PET/CT with a mean SUV_{max} of 16.6 ± 12.8

Table 1 Clinical characteristics of the patient cohort

Pt. No.	*SDHx* Mutation	Family History	Age (d)	Age (s)	LOP	Hypersecretion (Plasma)	TTM	LOM	Treatment received before scan	Treatment instituted after scan
1	***SDHB*, c.418G > T, p.Val140Phe**	Neg	11	13	R Adrenal	NE, NMN, DA, MTY, CgA	2	Abdomen	Surgical resection	Surgical resection
2	***SDHA*, c.91C > T, p.Arg31X**	Neg	14	15	R Retroperitoneal	DA, MTY	Metastatic at the time of initial diagnosis	Bones	Surgical resection	Surgical resection, PRRT with ^{90}Y–DOTATOC therapy
3	***SDHD*, c.388dupG, p.130 fs**; *SDHB* variant, c.423 + 20 T > A (intronic point mutation)	Pos	16	16	L Carotid body	Silent	Metastatic at the time of initial diagnosis	Abdomen	None	Lost to f/u
4	***SDHB*, c.590C > G, p.Pro197Arg**	Pos	14	16	R Retroperitoneal	NE, NMN, MTY, CgA	Metastatic at the time of initial diagnosis	Bones	Surgical resection	MIBG
5	***SDHB*, c.418G > T, p.Val140Phe**	Neg	8	16	Mediastinum	NE, NMN	2	Mediastinum, Abdomen, Bones	Surgical resection, MIBG	Bisphosphonate
6	***SDHB*, c.418G > T, p.Val140Phe**	Pos	15	16	Bladder	CgA	Metastatic at the time of initial diagnosis	Lymph nodes	Surgical resection	None
7	***SDHB*, c.1_72del**	Pos	8	10	R Paraaortic/ Retroperitoneal	NE, NMN, CgA	Metastatic at the time of initial diagnosis	Abdomen, Lungs, Bone	Surgical resection	PRRT with ^{177}Lu-DOTATATE
8	***SDHB*, c.725G > A, p.Arg242His**	Neg	14	16	R carotid body	NE, NMN, DA, MTY, CgA	Metastatic at the time of initial diagnosis	Abdomen, Bones	Surgical resection	Bisphosphonate
9	***SDHB*, c.72 + 1G > T, IVS1 + 1G > T**	Pos	10	14	R Retroperitoneal	NE, NMN	Metastatic at the time of initial diagnosis	Abdomen, Lungs, Liver, Bone	Surgical resection	Lost to f/u

*mutation highlighted in bold is the pathogenic/likely pathogenic mutation

Abbreviations: Age (d), age in years at diagnosis; Age (s), age in years at the time of ^{68}Ga-DOTATATE scan; CgA, chromogranin A; DA, dopamine; f/u, follow-up; fs, frameshift mutation; L, left; LOM, location of metastasis; LOP, location of primary; MTY, methoxytyramine; N/A, not applicable; Neg, negative; NE, norepinephrine; NMN, normetanephrine; Pos, positive; PRRT, peptide receptor radionuclide therapy; R, right; TTM, time in years for metastasis

(median: 14.0; range: 2.1 to 61.3), corresponding to 79.4% of lesions (95% CI, 70.5% to 86.6%; $p = 0.001$). CT/MR imaging detected 79 of the 107 lesions, corresponding to 73.8% of lesions (95% CI, 64.5% to 81.9%; $p < 0.001$).

Lesion-based detection performance of ^{68}Ga-DOTATATE PET/CT compared with ^{18}F–FDG PET/CT and CT/MR imaging stratified per various anatomic regions are as follows (Tables 2 and 3). In the neck and the lungs, the per-lesion detection rate was similar for ^{68}Ga-DOTATATE PET/CT, ^{18}FDG PET/CT, and CT/MR imaging. In contrast to ^{68}Ga-DOTATATE PET/CT and CT/MR imaging, ^{18}FDG PET/CT was unable to detect any adrenal and liver lesions, whereas for other abdominal lesions, ^{18}FDG PET/CT and CT/MR imaging had a similar per-lesion detection rate, better than that of ^{68}Ga-DOTATATE PET/CT. In the mediastinum, the per-lesion detection rate was similar for ^{68}Ga-DOTATATE PET/CT and ^{18}FDG PET/CT, better than that of CT/MR imaging whereas for the bone lesions, ^{68}Ga-DOTATATE PET/CT performed better than both ^{18}FDG PET/CT and CT/MR imaging.

All eight patients with abnormal findings detected on imaging studies had metastases that were located in the mediastinum, lungs, liver, abdomen/pelvis, and/or bones. A lesion-based evaluation excluding the patient with ^{18}F–FDG PET/MR scan did not result in any significant statistical change.

In 6 patients, a total of seven lesions, five abdominal and two bone lesions, were not visualized on ^{68}Ga-DOTATATE PET/CT. Of those seven lesions, one lesion was retrospectively present on a second look/review. Two lesions, one bone and one abdominal lymph node in two patients, which were missed on ^{68}Ga-DOTATATE PET/CT were detected on ^{18}F–FDG PET/CT studies. The remaining four lesions, three abdominal lymph nodes and a bone lesion in three patients were positive only on CT/MR imaging, and one lesion, an abdominal lymph node of a patient, was positive on both ^{18}F–FDG PET/CT and CT/MR imaging studies.

Eleven bone lesions in three patients were identified only on ^{68}Ga-DOTATATE PET/CT with a mean SUV_{max} of 7.8 ± 4.9 (median: 6.5; range: 2 to 19.2). The mean size of the four lesions that were positive only on CT/MR imaging was 0.6 cm ± 0.2 cm (median: 0.5; range: 0.4 to 0.9 cm), whereas mean size calculated from PET images for the 11 lesions positive only on ^{68}Ga-DOTATATE PET/CT was 0.7 cm ± 0.2 cm (median: 0.7; range: 0.4 to 0.9 cm) and that of two lesions positive only on ^{18}F–FDG PET was 0.6 cm ± 0.1 cm (median:0.6; range: 0.5 and 0.7 cm).

The per-region detection rates for ^{68}Ga-DOTATATE PET/CT was 100% (95% CI: 84.6 to 100) identifying all 22 of 22 involved regions. It was 90.9% (95% CI, 70.8% to 98.9%) for both ^{18}F–FDG PET/CT and CT/MR imaging identifying 20 of 22 involved regions. The per-patient detection rates for ^{68}Ga-DOTATATE PET/CT, ^{18}FDG PET/CT, and CT/MR imaging were all 100% (95% CI, 63.1% to 100%) identifying eight out of the involved eight patients.

Based on their intense ^{68}Ga-DOTATATE lesion-uptake, two of our patients who had *SDHB* mutations and extensive metastasis (Table 1, patients 2 and 7) were treated with PRRT, receiving ^{90}Y–DOTATOC and ^{177}Lu-DOTATATE, respectively.

The per-lesion, per-region and per-patient results are summarized in Table 4. Representative PET images comparing ^{68}Ga-DOTATATE and ^{18}F–FDG PET/CT are shown in Figs. 2 and 3.

Discussion

To the best of our knowledge, this is the first study that provides a head-to-head comparison of ^{68}Ga-DOTATATE PET/CT, ^{18}F–FDG PET/CT and CT/MR imaging for localizing *SDHx*-related PPGLs in pediatric patients.

Functional imaging agents target different mechanisms of tumorigenesis in PPGLs. Similar to other NETs, PPGLs are known to express somatostatin receptors (SSTR) especially SSTR2 subtype [24]; ^{68}Ga-DOTATATE is known to demonstrate higher affinity for SSTR2 [25]. Initially, in our protocol,^{68}Ga-DOTATATE PET/CT was approved only in adult patients, which precluded pediatric patients from undergoing ^{68}Ga-DOTATATE PET/CT for the evaluation of PPGLs. However, encouraged by the superior diagnostic performance of ^{68}Ga-DOTATATE PET/CT to other functional imaging modalities in adult *SDHB*-related metastatic PPGLs [22], sporadic metastatic PPGLs [26], and head and neck PGLs [27], our protocol was amended and children between 10 to 18 years of age were allowed to undergo ^{68}Ga-DOTATATE PET/CT for the evaluation of PPGLs. In this population, we decided to study first the diagnostic performance of ^{68}Ga-DOTATATE PET/CT in *SDHx*-related PPGLs, which are known to be more aggressive than those with other genetic mutations, and which have a higher rate of metastatic disease with limited treatment options, thus a poor prognosis.

In our study, ^{68}Ga-DOTATATE PET/CT with a per-lesion detection rate of 93.5% demonstrated significantly higher detection rate compared to ^{18}F–FDG PET/CT and CT/MR imaging. This finding is similar to the results reported recently in localization of *SDHB*-related adult metastatic PPGLs with ^{68}Ga-DOTATATE PET/CT, where it showed a slightly higher detection rate, 98.9% [22]. However, in our pediatric cohort, performance of ^{68}Ga-DOTATATE PET/CT for the detection of abdominal PPGLs was suboptimal with a rate of 66.7%, compared to both ^{18}F–FDG PET/CT and CT/MR imaging, which showed a detection rate of 80%. This finding is in contrast to the results obtained in 17 adult patients with metastatic *SDHB* mutation where ^{68}Ga-DOTATATE PET/CT detected 100% of abdominal PPGLs [22]. However, our findings are in agreement with the recently published results in a mixed

Table 2 Number of identified lesions in ^{68}Ga-DOTATATE PET/CT, ^{18}F–FDG PET/CT, and CT/MR imaging compared to lesions identified by the imaging comparator based on lesion location

Lesions	^{68}Ga-DOTATATE PET/CT	^{18}F–FDG PET/CT	CT/MR
All compartments	[a]100/107	85/107	79/107
Neck	3/3	3/3	3/3
Mediastinum	5/5	5/5	0/5
Lungs	17/17	17/17	17/17
Adrenal	1/1	0/1	1/1
Liver	2/2	0/2	2/2
Abdomen	[b]10/15	12/15	12/15
Bone	62/64	48/64	44/64

[a] 105/107 if CT/MR imaging of the abdomen is combined with ^{68}Ga-DOTATATE PET/CT. [b] 14/15 if CT/MR imaging of the abdomen/pelvis is combined with ^{68}Ga-DOTATATE PET/CT

small cohort of four pediatric patients with PPGLs with and without germline mutations, where the detection rate of ^{68}Ga-DOTATATE PET/CT in localization of abdominal PPGLs was 60% [14]. A possible explanation is reduced expression of SSTR2 in pediatric abdominal PPGLs resulting in a suboptimal performance of ^{68}Ga-DOTATATE PET/CT in detection of abdominal PPGLs. Thus, future studies in larger pediatric cohorts are warranted. It is to be noted that the use of CT/MR imaging along with ^{68}Ga-DOTATATE PET/CT further aid in the detection of four out of five missed abdominal lesions on ^{68}Ga-DOTATATE PET/CT, resulting in the improved overall detection of 93.3% (14/15) of abdominal lesions. This provides a strong evidence of performing CT/MR imaging along with ^{68}Ga-DOTATATE PET/CT or performing the CT portion of ^{68}Ga-DOTATATE PET/CT as contrast-enhanced CT to complement the lesion detection of pediatric *SDHx*-related abdominal PPGLs by ^{68}Ga-DOTATATE PET/CT thereby further improving the diagnostic power of ^{68}Ga-DOTATATE PET/CT.

The detection of primary and metastatic PPGLs with ^{68}Ga-DOTATATE PET/CT in pediatric patients can play a significant role in their medical management, not only because of its diagnostic accuracy, but also to determine patients' eligibility for PRRT and/or cold somatostatin analog therapy. DOTA peptides, such as DOTATATE and DOTATOC, labeled with therapeutic beta emitters such as ^{177}Lutetium (^{177}Lu) and ^{90}Yttrium (^{90}Y) is used in PRRT. Thus, ^{68}Ga-DOTATATE PET/CT can also be used to determine patients' potential eligibility for PRRT using ^{177}Lu-DOTATATE (Lutathera®) [28], since the treatment options in pediatric patients with metastatic PPGLs are limited. For example, two of our patients (Table 1, patients 2 and 7) based on their intense ^{68}Ga-DOTATATE lesion-uptake, were treated with PRRT, receiving ^{90}Y–DOTATOC and ^{177}Lu-DOTATATE, respectively.

In comparison with normal cells, increased glucose metabolism of the tumor cells is the hallmark of cancer imaging with ^{18}F–FDG PET/CT. Increased ^{18}F–FDG uptake is observed in *SDHx*-related PPGLs and metastatic tumors due to altered

Table 3 Detection rate (%) and 95% CI (%) for ^{68}Ga-DOTATATE PET/CT, ^{18}F–FDG PET/CT, and CT/MR imaging based on lesion location

Lesion location	^{68}Ga-DOTATATE PET/CT		^{18}F–FDG PET/CT		CT/MR	
	Detection rate (%)	95% CI (%)	Detection rate (%)	95% CI (%)	Detection rate (%)	95% CI (%)
All compartments	[a]93.5	87.0–97.3	79.4	70.5–86.6	73.8	64.5–81.9
Neck	100	29.2–100	100	29.2–100	100	29.2–100
Mediastinum	100	47.8–100	100	47.8–100	0	0.0–52.2
Lungs	100	80.5–100	100	80.5–100	100	80.5–100
Adrenal	100	2.5–100	0	0.0–97.5	100	2.5–100
Liver	100	15.8–100	0	0.0–84.2	100	15.8–100
Abdomen	[b]66.7	38.4–88.2	80	51.9–95.7	80	51.9–95.7
Bone	96.9	89.2–99.6	75	62.6–85.0	68.8	55.9–79.8

[a] 98.4% (95% CI, 93.4% to 99.8%) if CT/MR imaging of the abdomen/pelvis is combined with ^{68}Ga-DOTATATE PET/CT. [b] 93.3% (95% CI, 68.1% to 99.8%) if CT/MR imaging of the abdomen/pelvis is combined with ^{68}Ga-DOTATATE PET/CT

Table 4 Per-lesion, per-region, per-patient detection rate (%) and 95% CI (%) for ^{68}Ga-DOTATATE PET/CT, ^{18}F–FDG PET/CT, and CT/MR imaging

Detection rate	^{68}Ga-DOTATATE PET/CT		^{18}F–FDG PET/CT		CT/MR	
	Detection rate (%)	95% CI (%)	Detection rate (%)	95% CI (%)	Detection rate (%)	95% CI (%)
Per - lesion	[a]93.5 (100/107)	87.0–97.3	79.4 (85/107)	70.5–86.6	73.8 (79/107)	64.5–81.9
Per - region	100 (22/22)	84.6–100	90.9 (20/22)	70.8–98.9	90.9 (20/22)	70.8–98.9
Per - patient	100 (8/8)	63.1–100	100 (8/8)	63.1–100	100 (8/8)	63.1–100

Values in parentheses are the ratio of the number of lesions, regions, or patients detected by imaging modality to that by the imaging comparator

[a] 98.4% (105/107) (95% CI, 93.4% to 99.8%) if CT/MR imaging of the abdomen/pelvis is combined with ^{68}Ga-DOTATATE PET/CT

glucose metabolism, which is related to genotype-specific tumor biology [12, 29]. In our pediatric cohort, the per-lesion detection rate of ^{18}F–FDG PET/CT is 79.4%, which is slightly lower than the previously reported rate of 85.8% obtained in a 17 patient-cohort of *SDHB*-related metastatic adult PPGLs patients [22]. This slight lower rate of lesion detection rate for ^{18}F–FDG PET/CT, at least in part, might be attributable to the challenges that ^{18}F–FDG PET/CT studies poses in children. Such difficulties include several age-dependent normal physiologic variations like ^{18}F–FDG uptake in the thymus, increased activity in skeletal growth centers, extensive distribution of hematopoietic bone marrow, and activated brown adipose tissue related variant biodistribution of ^{18}F–FDG activity [30, 31]. For example, in two patients, we noted intense ^{18}F–FDG uptake in activated brown adipose tissue. In one of these two patients, detection of a recurrent lesion present in the adrenal bed was missed due to surrounding extensive and intense ^{18}F–FDG uptake of the activated brown adipose tissue

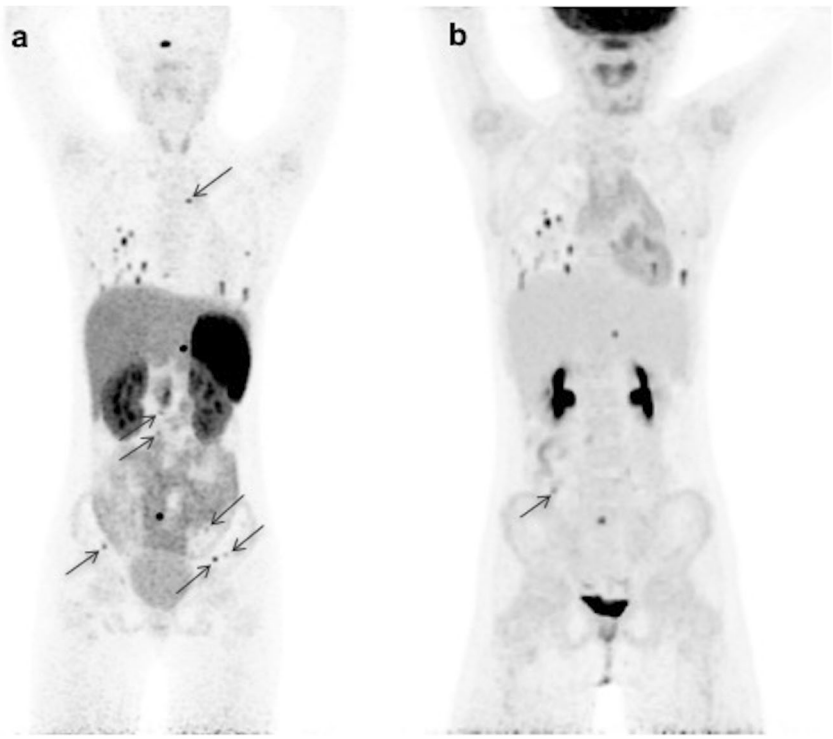

Fig. 2 Anterior MIP (maximal intensity projection) images of the ^{68}Ga-DOTATATE PET/CT (a) and ^{18}F–FDG PET/CT (b) studies of a 10-year-old *SDHB* positive girl (patient no. 7 in Table 1) with metastatic PPGL. She was diagnosed initially with metastatic disease at the age of 8 years. Her right paraaortic, retroperitoneal primary PGL then was surgically resected. On presentation to our institution, the progression of her disease showed avid metastatic lesions in her lungs, abdomen, and bone by tracers, as seen in the images a and b. All the additional lesions (transverse process of T4 spine, L2-L5 vertebral bodies, left ilium, and left and right iliac wings) localized by the ^{68}Ga-DOTATATE PET/CT that are not visualized by ^{18}F–FDG PET/CT are marked by arrows on image (a), and similarly the single arrow on image (b), indicates the one lesion (abutting bowel) localized by ^{18}F–FDG PET/CT that is not visualized by the ^{68}Ga-DOTATATE PET/CT

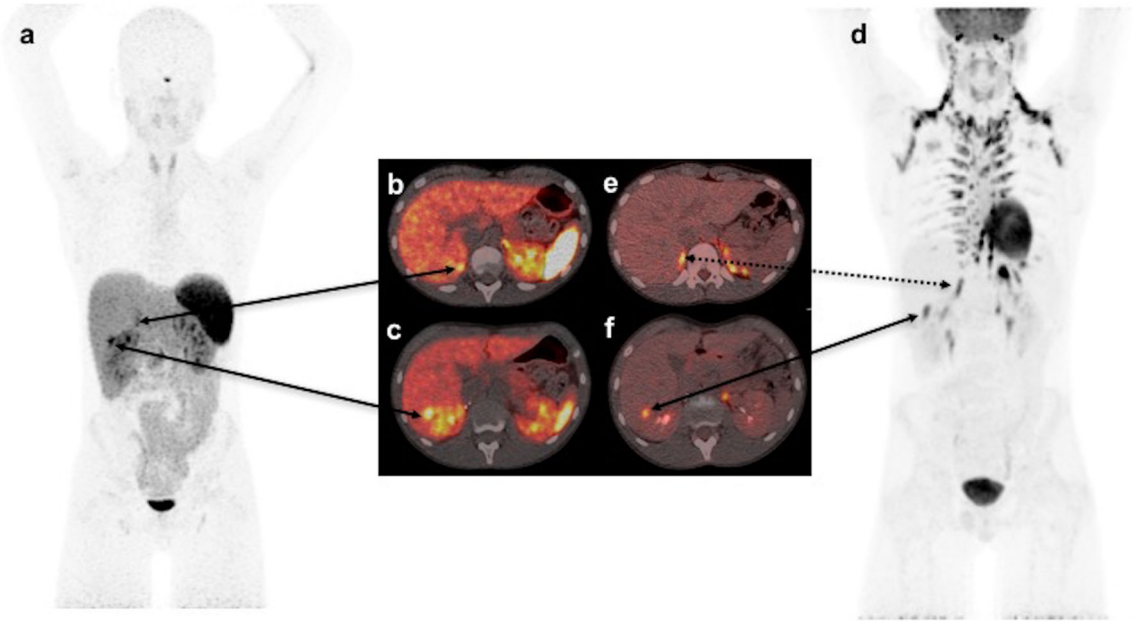

Fig. 3 Anterior MIP images of ^{68}Ga-DOTATATE PET/CT (a) and ^{18}F–FDG PET/CT (d) study of a 13-year-old *SDHB* positive boy with metastatic PPGL (patient no. 1 in Table 1). He was diagnosed initially with right adrenal pheochromocytoma at the age of 11 years, for which he underwent a partial right adrenalectomy. Fused ^{68}Ga-DOTATATE PET and CT (b and c) and fused ^{18}F–FDG PET and CT (e and f) transaxial sections through the same malignant lesions depicted on MIP images of ^{68}Ga-DOTATATE PET/CT (a) and ^{18}F–FDG PET/CT (d), respectively, on his current presentation. Those two new malignant lesions detected on the ^{68}Ga-DOTATATE PET/CT (a) study are represented by solid arrows: first located at right adrenal postsurgical bed (b), and the second inferior lesion located superolateral to the upper pole of the right kidney. On the initial interpretation of the ^{18}F–FDG PET/CT (d) study, only one of the two lesions depicted on ^{68}Ga-DOTATATE PET/CT study (c), was identified on ^{18}F–FDG PET/CT (f) study, located at superolateral to the upper pole of the right kidney. The second lesion (e) depicted by dashed arrows, located at right adrenal postsurgical bed initially is not recognized as a malignant lesion due to the presence of intensely increased normal-variant ^{18}F–FDG uptake of the activated brown adipose tissue obscuring its detection. When the ^{18}F–FDG PET/CT study was re-reviewed with the knowledge of the findings of his ^{68}Ga-DOTATATE PET/CT study, although initially was missed, the second lesion was perceived as noticeable. Subsequently, the patient underwent resection of these two lesions which were confirmed to be PGL on the histopathologic examination

(Fig. 3). Needless to say, more cautious interpretation is warranted while interpreting ^{18}F–FDG PET/CT studies of pediatric patients with activated brown adipose tissue.

There are several limitations of this study. First, the study cohort is relatively small. However, considering the extreme rarity of PPGLs in pediatric age group, which is 0.02 cases per million children for malignant PPGLs [15], and the scarcity of information on advanced functional imaging modalities available in the scientific literature, it becomes imperative to report findings obtained from even small study cohort. Second, due to retrospective nature of the study and our institution being a tertiary research center and hence, this study may have inherent biases including referral bias. Third, in keeping with the institutional imperative to limit radiation exposure of children, ^{18}F–fluorodopa PET/CT could not be included in the study design in which advanced functional imaging studies and anatomic imaging modalities undergo head-to-head comparison. Fourth, in an attempt to keep the radiation doses to ALARA level, in one patient ^{18}F–FDG PET/CT was not performed as she presented to us with ^{18}F–FDG PET/MR. However, no significant difference in calculated detection rates was observed even when this case was excluded from calculations. Similarly, anatomic imaging was not repeated in those patients who had already obtained anatomic imaging at an outside institution.

Conclusion

Based on our relatively small cohort of pediatric patients, the detection rate of *SDHx*-related PPGLs with ^{68}Ga-DOTATATE PET/CT is superior to CT/MR imaging and ^{18}F–FDG PET/CT, which is the currently recommended functional imaging modality in this population with the exception of abdominal (excluding adrenal and liver) lesions. Further, performing contrast-enhanced ^{68}Ga-DOTATATE PET/CT would improve the diagnostic power of ^{68}Ga-DOTATATE PET/CT. Based on these findings, contrast-enhanced ^{68}Ga-DOTATATE PET/CT or PET/MR might emerge as the standard for detection of *SDHx*-related PPGLs in the pediatric population.

The treatment options in pediatric patients with metastatic PPGLs are very limited. In addition to their superiority as an imaging agent, DOTA peptides, such as DOTATATE, can

also be labeled with therapeutic beta emitters such as ^{177}Lu and ^{90}Y. Thus, patients' ^{68}Ga-DOTATATE PET/CT studies can also be used to determine their potential eligibility for PRRT.

Acknowledgements We would like to thank Dr. Paul Wakim for the assistance in statistical analyses. We would also like to thank the patients and their families, for participating in the study, and all of the people who participated in this project, especially the technologists in the NIH Clinical Center PET Department.

Financial disclosure This work was supported, in part, by the Intramural Research Program of the National Institutes of Health, *Eunice Kennedy Shriver* National Institute of Child Health and Human Development and was supported, in part, by the Intramural Research Program of the Center for Cancer Research, National Cancer Institute.

Compliance with ethical standards

Funding This study was funded by National Institutes of Health (grant number: Z1AHD008735).

Conflict of interest Author Abhishek Jha declares no conflict of interest. Author Alexander Ling declares no conflict of interest. Author Corina Millo declares no conflict of interest. Author Garima Gupta declares no conflict of interest. Author Bruna Viana declares no conflict of interest. Author Frank I. Lin declares no conflict of interest. Author Peter Herscovitch declares no conflict of interest. Author Karen T. Adams declares no conflict of interest. Author David Taïeb declares no conflict of interest. Author Adam R. Metwalli declares no conflict of interest. Author W. Marston Linehan declares no conflict of interest. Author Alessandra Brofferio declares no conflict of interest. Author Constantine A. Stratakis declares no conflict of interest. Author Electron Kebebew declares no conflict of interest. Author Maya Lodish declares no conflict of interest. Author Ali Cahid Civelek declares no conflict of interest. Author Karel Pacak declares no conflict of interest. Informed consent was obtained from all individual participants included in the study.

Ethical approval All procedures performed in studies involving human participants were in accordance with the ethical standards of the institutional and/or national research committee and with the 1964 Helsinki declaration and its later amendments or comparable ethical standards.

Informed consent Informed assent from the patients and signed permission from one or both parents were obtained for all the individual participants included in the study.

References

1. Schiffman JD. No child left behind in SDHB testing for paragangliomas and pheochromocytomas. J Clin Oncol. 2011;29:4070–2. https://doi.org/10.1200/JCO.2011.37.8695.
2. Neumann HP, Bausch B, McWhinney SR, Bender BU, Gimm O, Franke G, et al. Germ-line mutations in nonsyndromic pheochromocytoma. N Engl J Med. 2002;346:1459–66. https://doi.org/10.1056/NEJMoa020152.
3. Neumann HP, Pawlu C, Peczkowska M, Bausch B, McWhinney SR, Muresan M, et al. Distinct clinical features of paraganglioma syndromes associated with SDHB and SDHD gene mutations. JAMA. 2004;292:943–51. https://doi.org/10.1001/jama.292.8.943.
4. Burnichon N, Briere JJ, Libe R, Vescovo L, Riviere J, Tissier F, et al. SDHA is a tumor suppressor gene causing paraganglioma. Hum Mol Genet. 2010;19:3011–20. https://doi.org/10.1093/hmg/ddq206.
5. Bayley JP, Kunst HP, Cascon A, Sampietro ML, Gaal J, Korpershoek E, et al. SDHAF2 mutations in familial and sporadic paraganglioma and phaeochromocytoma. Lancet Oncol. 2010;11:366–72. https://doi.org/10.1016/S1470-2045(10)70007-3.
6. Michalowska I, Cwikla JB, Peczkowska M, Furmanek MI, Buscombe JR, Michalski W, et al. Usefulness of somatostatin receptor scintigraphy (Tc-[HYNIC, Tyr3]-octreotide) and 123I-Metaiodobenzylguanidine scintigraphy in patients with SDHx gene-related Pheochromocytomas and Paragangliomas detected by computed tomography. Neuroendocrinology. 2015;101:321–30. https://doi.org/10.1159/000381458.
7. Bezawork-Geleta A, Rohlena J, Dong L, Pacak K, Neuzil J. Mitochondrial Complex II: At the Crossroads. Trends Biochem Sci. 2017;42:312–325. doi:https://doi.org/10.1016/j.tibs.2017.01.003.
8. Ayala-Ramirez M, Feng L, Johnson MM, Ejaz S, Habra MA, Rich T, et al. Clinical risk factors for malignancy and overall survival in patients with pheochromocytomas and sympathetic paragangliomas: primary tumor size and primary tumor location as prognostic indicators. J Clin Endocrinol Metab. 2011;96:717–25. https://doi.org/10.1210/jc.2010-1946.
9. Turkova H, Prodanov T, Maly M, Martucci V, Adams K, Widimsky J Jr, et al. Characteristics and outcomes of metastatic Sdhb and sporadic Pheochromocytoma/Paraganglioma: an National Institutes of Health study. Endocr Pract. 2016;22:302–14. https://doi.org/10.4158/EP15725.OR.
10. Benn DE, Gimenez-Roqueplo AP, Reilly JR, Bertherat J, Burgess J, Byth K, et al. Clinical presentation and penetrance of pheochromocytoma/paraganglioma syndromes. J Clin Endocrinol Metab. 2006;91:827–36. https://doi.org/10.1210/jc.2005-1862.
11. Amar L, Baudin E, Burnichon N, Peyrard S, Silvera S, Bertherat J, et al. Succinate dehydrogenase B gene mutations predict survival in patients with malignant pheochromocytomas or paragangliomas. J Clin Endocrinol Metab. 2007;92:3822–8. https://doi.org/10.1210/jc.2007-0709.
12. Timmers HJ, Chen CC, Carrasquillo JA, Whatley M, Ling A, Eisenhofer G, et al. Staging and functional characterization of pheochromocytoma and paraganglioma by 18F-fluorodeoxyglucose (18F-FDG) positron emission tomography. J Natl Cancer Inst. 2012;104:700–8. https://doi.org/10.1093/jnci/djs188.
13. Parenti G, Zampetti B, Rapizzi E, Ercolino T, Giache V, Mannelli M. Updated and new perspectives on diagnosis, prognosis, and therapy of malignant pheochromocytoma/paraganglioma. J Oncol. 2012;2012:872713. https://doi.org/10.1155/2012/872713.
14. Babic B, Patel D, Aufforth R, Assadipour Y, Sadowski SM, Quezado M, et al. Pediatric patients with pheochromocytoma and paraganglioma should have routine preoperative genetic testing for common susceptibility genes in addition to imaging to detect extra-adrenal and metastatic tumors. Surgery. 2017;161:220–7. https://doi.org/10.1016/j.surg.2016.05.059.
15. Edmonds S, Fein DM, Gurtman A. Pheochromocytoma. Pediatr Rev. 2011;32:308–10. https://doi.org/10.1542/pir.32-7-308.
16. Ciftci AO, Tanyel FC, Senocak ME, Buyukpamukcu N. Pheochromocytoma in children. J Pediatr Surg. 2001;36(3):447–52. https://doi.org/10.1053/jpsu.2001.21612.
17. Barontini M, Levin G, Sanso G. Characteristics of pheochromocytoma in a 4- to 20-year-old population. Ann N Y Acad Sci. 2006;1073:30–7. https://doi.org/10.1196/annals.1353.003.
18. King KS, Prodanov T, Kantorovich V, Fojo T, Hewitt JK, Zacharin M, et al. Metastatic pheochromocytoma/paraganglioma related to primary tumor development in childhood or adolescence:

significant link to SDHB mutations. J Clin Oncol. 2011;29:4137–42. https://doi.org/10.1200/JCO.2011.34.6353.
19. Robbins E. Radiation risks from imaging studies in children with cancer. Pediatr Blood Cancer. 2008;51:453–7. https://doi.org/10.1002/pbc.21599.
20. Fahey FH, Treves ST, Adelstein SJ. Minimizing and communicating radiation risk in pediatric nuclear medicine. J Nucl Med. 2011;52:1240–51. https://doi.org/10.2967/jnumed.109.069609.
21. Lenders JW, Duh QY, Eisenhofer G, Gimenez-Roqueplo AP, Grebe SK, Murad MH, et al. Pheochromocytoma and paraganglioma: an endocrine society clinical practice guideline. J Clin Endocrinol Metab. 2014;99:1915–42. https://doi.org/10.1210/jc.2014-1498.
22. Janssen I, Blanchet EM, Adams K, Chen CC, Millo CM, Herscovitch P, et al. Superiority of [68Ga]-DOTATATE PET/CT to other functional imaging modalities in the localization of SDHB-associated metastatic Pheochromocytoma and Paraganglioma. Clin Cancer Res. 2015;21:3888–95. https://doi.org/10.1158/1078-0432.CCR-14-2751.
23. U.S. Food and Drug Administration. FDA approves new diagnostic imaging agent to detect rare neuroendocrine tumors. 2016. https://www.fda.gov/newsevents/newsroom/pressannouncements/ucm504524.htm. Accessed 05/30/2017.
24. Reubi JC, Waser B, Schaer JC, Laissue JA. Somatostatin receptor sst1-sst5 expression in normal and neoplastic human tissues using receptor autoradiography with subtype-selective ligands. Eur J Nucl Med. 2001;28:836–46.
25. Reubi JC, Schar JC, Waser B, Wenger S, Heppeler A, Schmitt JS, et al. Affinity profiles for human somatostatin receptor subtypes SST1-SST5 of somatostatin radiotracers selected for scintigraphic and radiotherapeutic use. Eur J Nucl Med. 2000;27:273–82.
26. Janssen I, Chen CC, Millo CM, Ling A, Taieb D, Lin FI, et al. PET/CT comparing (68)Ga-DOTATATE and other radiopharmaceuticals and in comparison with CT/MRI for the localization of sporadic metastatic pheochromocytoma and paraganglioma. Eur J Nucl Med Mol Imaging. 2016;43:1784–91. https://doi.org/10.1007/s00259-016-3357-x.
27. Janssen I, Chen CC, Taieb D, Patronas NJ, Millo CM, Adams KT, et al. 68Ga-DOTATATE PET/CT in the localization of head and neck Paragangliomas compared with other functional imaging modalities and CT/MRI. J Nucl Med. 2016;57:186–91. https://doi.org/10.2967/jnumed.115.161018.
28. Kong G, Grozinsky-Glasberg S, Hofman MS, Callahan J, Meirovitz A, Maimon O, et al. Efficacy of peptide receptor radionuclide therapy (PRRT) for functional metastatic Paraganglioma and Phaeochromocytoma. J Clin Endocrinol Metab. 2017; https://doi.org/10.1210/jc.2017-00816.
29. Favier J, Briere JJ, Burnichon N, Riviere J, Vescovo L, Benit P, et al. The Warburg effect is genetically determined in inherited pheochromocytomas. PLoS One. 2009;4:e7094. https://doi.org/10.1371/journal.pone.0007094.
30. Biermann M, Schwarzlmuller T, Fasmer KE, Reitan BC, Johnsen B, Rosendahl K. Is there a role for PET-CT and SPECT-CT in pediatric oncology? Acta Radiol. 2013;54:1037–45. https://doi.org/10.1258/ar.2012.120616.
31. Culverwell AD, Scarsbrook AF, Chowdhury FU. False-positive uptake on 2-[(1)(8)F]-fluoro-2-deoxy-D-glucose (FDG) positron-emission tomography/computed tomography (PET/CT) in oncological imaging. Clin Radiol. 2011;66:366–82. https://doi.org/10.1016/j.crad.2010.12.004.